

# Controlling mechanism of absence seizures by deep brain stimulus applied on subthalamic nucleus

Bing Hu<sup>1</sup> · Yu Guo<sup>1</sup> · Xiaoqiang Zou<sup>1</sup> · Jing Dong<sup>1</sup> · Long Pan<sup>1</sup> · Min Yu<sup>1</sup> · Zhejia Yang<sup>1</sup> · Chaowei Zhou<sup>1</sup> · Zhang Cheng<sup>1</sup> · Wanyue Tang<sup>1</sup> · Haochen Sun<sup>1</sup>

Received: 29 January 2017/Revised: 14 September 2017/Accepted: 11 October 2017  
© Springer Science+Business Media B.V. 2017

**Abstract** Based on a classical model of the basal ganglia thalamocortical network, in this paper, we employed a type of the deep brain stimulus voltage on the subthalamic nucleus to study the control mechanism of absence epilepsy seizures. We found that the seizure can be well controlled by turning the period and the duration of current stimulation into suitable ranges. It is the very interesting bidirectional periodic adjustment phenomenon. These parameters are easily regulated in clinical practice, therefore, the results obtained in this paper may further help us to understand the treatment mechanism of the epilepsy seizure.

**Keywords** SWDs · Subthalamic nucleus · DBS

## Introduction

Absence epilepsy is one kind of generalized non-convulsive brain seizure disease, mainly occurred in childhood (Loiseau et al. 1995). The typical features of absence seizures are transient loss of consciousness, and then suddenly stop, at the same time, along with the specific electrophysiological characteristics, i.e., bilateral synchronous spike wave discharges (SWDs) with slow oscillation frequency (2–4 Hz) (Loiseau et al. 1995; Crunelli and Leresche 2002), which

usually shown on the electroencephalogram (EEG) [which also used to check other brain nerve diseases, such as the Parkinson's disease (Yi et al. 2017)] of patients. The brain anatomical structure and medical experiments have shown that the SWDs of absence seizures mainly induced by abnormal interactions between the cortex and thalamus neurons, they form the cortical–thalamic (CT) loop system. The CT network is an important anatomical structure of the brain, the firing activity of which is closely related to the neurophysiological state of the brain, such as sleep, epilepsy seizure, etc. The physiological activity record of the cerebral cortex and thalamus on rodent models and clinical patients is the direct evidence of epileptic seizure arising from the CT system (Marescaux and Vergnes 1995; Coenen and Luijcklaar 2003). Subsequently, there have developed many concepts on the pathophysiology of epilepsy, such as the cortical focus theory (Meeren et al. 2005). At present, there are also many mathematical models, especially the mean field model, used to study the pathogenesis of epilepsy and have obtained a series of results are in good agreement with experiments (Robinson et al. 2002; Rodrigues et al. 2006, 2009; Takeshita et al. 2007; Marten et al. 2009a, b; Wilson et al. 2006; Case and Soltesz 2011; Dadok et al. 2012; Chen et al. 2014, 2015; Hu et al. 2015; Hu and Wang 2015; Hu et al. 2017; Paz et al. 2011; Paz and Huguenard 2015). Breakspear et al. employed the bifurcation analysis to give an unifying mechanism of primary generalized seizures (Breakspear et al. 2006). The detailed cellular and network mechanisms of genetically-determined absence seizures referred to (Pinault and O'Brien 2005). The gap junctions also play an important role in the process of epileptic seizure (Volman et al. 2011). Volman and Perc found that the rewiring and forming of new links between neurons may greatly affect the generation of seizures (Volman and Perc 2010). Recently, Fan and Wang et al. discussed the disinhibition-induced

✉ Bing Hu  
djhubingst@163.com

<sup>1</sup> Institute of Applied Mathematics, Department of Mathematics and Statistics, College of Science, Huazhong Agricultural University, Wuhan 430070, China

transition mechanism between absence and tonic–clonic seizures in detail (Fan et al. 2015).

The basal ganglia, as a functional unit of the brain, mainly comprise of the striatum neurons, the substantia nigra pars reticulata (SNr) neurons, the globus pallidus external (GPe) segment neurons, the globus pallidus internal (GPi) segment neurons and the subthalamic nucleus (STN) neurons. From the perspective of anatomical structure, the basal ganglia have close input and output relationships with the thalamocortical system. It mainly receives excitatory signals from the cortex and thalamus, and in turn sends inhibitory projections to the thalamus. There have many studies indicated that the physiological activities of basal ganglia can crucially affect the onset of epilepsy disease (Deransart et al. 1998; Deransart and Depaulis 2002; Slaght et al. 2002; Rektor et al. 2013; Arakaki et al. 2016). Therefore, it is a natural idea to consider the basal ganglia as the therapeutic target to inhibit epileptic seizures, such as the deep brain stimulation (DBS) technology. There have many studies shown that the DBS acted on basal ganglia was very effective to control some brain nerve diseases, such as parkinson's disease (Cunha et al. 2015; Hemptinne et al. 2015; Fasano et al. 2015; Sweet et al. 2014; Wichmann and DeLong 2016). Though, there have also some researches implied that DBS acted on the STN (Chabards et al. 2002; Feng et al. 2014; Handforth et al. 2006; Lee et al. 2006) may also effective to control epilepsy, the theoretical mechanisms are still unclear and the related basal ganglia mathematical model study involved little.

The DBS is currently the main “invasive treatment” method of brain neural diseases (Krishnamurthi et al. 2012; Schtt and Claussen 2012), one of its main targets is the subthalamic nucleus (STN). A number of clinical and experimental studies have shown that this technique is very effective in the treatment of intractable epilepsy that is difficult to control with drugs (Rahman et al. 2010; Chambers and Bowen 2013; Vonck et al. 2013; Child et al. 2014; Paz et al. 2013; Krishna and Lozano 2014). For example, Handforth et al. pointed out that the bilateral subthalamic deep brain stimulation was efficacy and safety for treating the refractory partial-onset epilepsy (Handforth et al. 2006). Feng et al. studied a virally mediated transsynaptic tracing in transgenic mouse model, and found that stimulating the dorsal portion of subthalamic nucleus may be a viable therapeutic approach in pharmacoresistant epilepsy (Feng et al. 2014). There are also some theoretical model researches explored stimulus driven control mechanism of seizures. Such as, Taylor et al. (2014) based on real-time spike-wave position detection, developed an adaptive approach to find optimal stimulation parameters patient-specifically. Recently, Taylor et al. (2015) shown that optimal control protocols may be found for heterogeneous brain connectivity

of different patients, based on seizure abatement. Shan et al. (2015) explored the closed loop iterative learning control mechanism of epilepsy in a neural mass model. Sorokin et al. (2017) pointed out that rapid real-time switching between the phasic and tonic firing in thalamocortical neurons can realize bidirectional control of epileptic seizure. Recently, there are also some studies involved turning neuronal dynamics to appropriate rhythm, the results of which may closely relative to epileptic rhythm control. Such as, Guo et al. (2016) found that autaptic transmission of neurons can modulate irregular neuronal firings by turning the frequency of burst firing. And then, Guo et al. (2016b) explored the possible roles of autaptic inhibition in regulating the firing dynamics of fast-spiking interneurons. However, the treatment mechanism of deep brain stimulation is still unclear, especially, the research based on the mean-field mathematical theoretical model is seldom involved.

In this paper, based on a classical basal ganglia thalamocortical (BGCT) model (Chen et al. 2014, 2015; Hu et al. 2015; Hu and Wang 2015; Hu et al. 2017), we employed a type of the deep brain stimulus voltage on the STN to study the control mechanism of absence epilepsy seizures. We found that the seizure can be well controlled by turning the period (P) and the duration (D) of current stimulation into suitable ranges. It is the very interesting bidirectional periodic adjustment phenomenon. The data used in this paper are taken from real experiments, and the two parameters P and D may be both easily adjusted in clinical practice. Therefore, the results obtained can further help us to understand the therapeutic mechanism of epilepsy, might also have some guiding significance for the choice of clinical treatment scheme in future.

## Model and numerical calculation method

### The model introduced

In this section, we first give the schematic model in Fig. 1 (Chen et al. 2014, 2015; Hu et al. 2015; Hu and Wang 2015; Hu et al. 2017), which contains nine neural populations. In order to facilitate the following description, they are abbreviated as follows,  $e$  = excitatory pyramidal neurons (EPN);  $i$  = inhibitory interneurons (IIN);  $r$  = thalamic reticular nucleus (TRN);  $s$  = specific relay nuclei of thalamus (SRN);  $d_1$  = striatal D1 neurons;  $d_2$  = striatal D2 neurons;  $p_1$  = substantia nigra pars reticulata (SNr);  $p_2$  = globus pallidus external (GPe) segment;  $\zeta$  = subthalamic nucleus (STN). There are three types of synapse connections in the network, distinguished by different line types and heads in Fig. 1. The excitatory projections mediated by glutamate are represented by lines with arrows, and round heads mean inhibitory projections

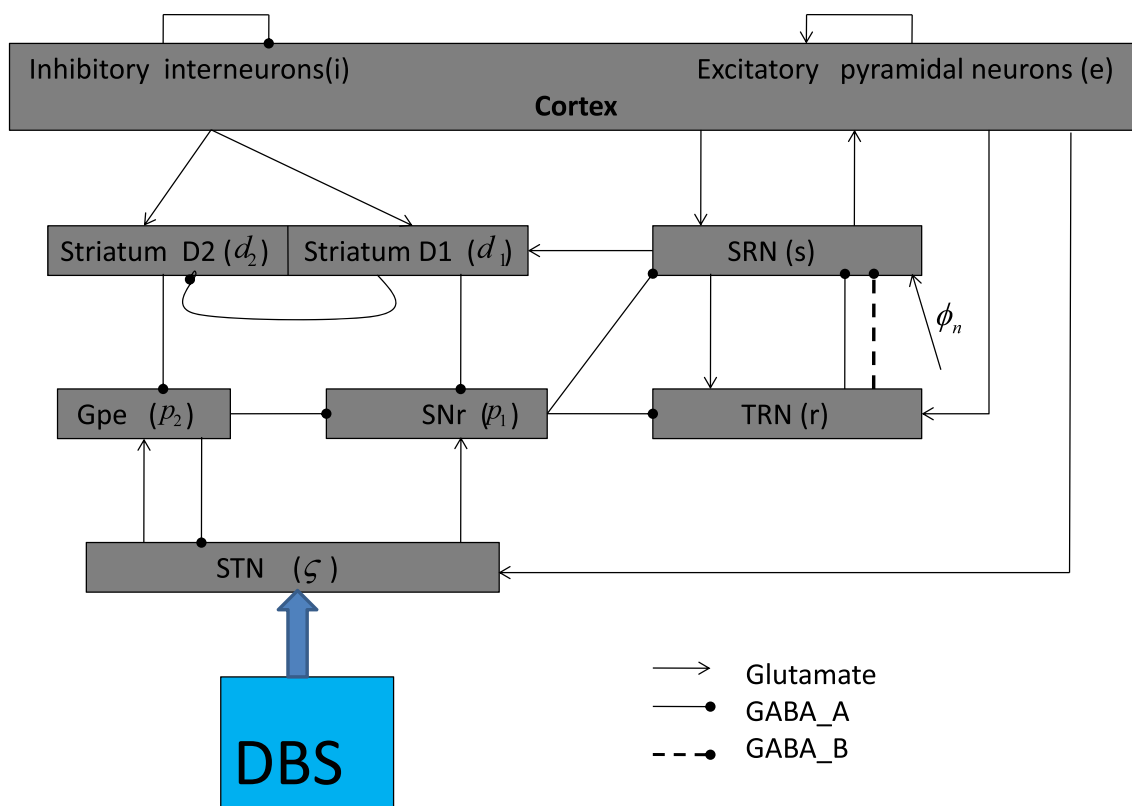


**Fig. 1** Schematic diagram of the employed basal ganglia–corticothalamic model. Nine neural populations are marked as,  $e$  = excitatory pyramidal neurons (EPN);  $i$  = inhibitory interneurons (IIN);  $r$  = thalamic reticular nucleus (TRN);  $s$  = specific relay nuclei (SRN);  $d_1$  = striatal D1 neurons;  $d_2$  = striatal D2 neurons;  $p_1$  = substantia nigra pars reticulata (SNr);  $p_2$  = globus pallidus external (GPe) segment;  $\zeta$  = subthalamic nucleus (STN). Lines ended with arrow

heads represent the excitatory projection; solid lines with round heads are the inhibitory projections mediated by the  $GABA_A$  receptor; the dashed line means the inhibitory output from TRN to SRN adjusted by the  $GABA_B$  receptor.  $\phi_n$  denotes the constant nonspecific subthalamic input onto SRN. DBS is the deep brain stimulation voltage acted on STN

regulated by  $GABA_A$  (solid line) and  $GABA_B$  (dotted line), respectively.  $I_{DBS} * R$  is the deep brain stimulation voltage, where, the  $I_{DBS}$  is the deep brain stimulation current,  $R$  is a fixed resistor, in order to simplify, we set  $R = 1 \text{ m}\Omega$  in the numerical calculation. In this paper, the current used is a common square wave stimulation current, a typical shape is illustrated in Fig. 2. The mathematical expression is as follows (Rubin and Terman 2004),

$$I_{DBS} = A \times H\left(\sin\left(\frac{2\pi t}{P}\right)\right) \left(1 - H\left(\frac{\sin(2\pi(t + D))}{P}\right)\right) \tag{1}$$

where  $H$  is a Heaviside step function, such that  $H(x) = 0$  if  $x < 0$  and  $H(x) = 1$  if  $x > 0$ .  $A$  is the amplitude of DBS current,  $P$  is the period of DBS current,  $D$  is the duration of positive input in one period.

By simplifying the mean field model, we can study the macroscopic dynamical behavior of each nerve population

effectively in the follow. Firstly, for each nerve nucleus “ $a$ ”, the dependency relation of the mean firing rate  $Q_a$  on the cell-body potential  $V_a$  is described as a sigmoid function curve (Albada et al. 2009; Albada and Robinson 2009b),

$$Q_a(t) \equiv F[V_a(t)] = \frac{Q_a^{max}}{1 + \exp\left[-\frac{\pi}{\sqrt{3}} \frac{V_a(t) - \theta_a}{\sigma}\right]} \tag{2}$$

where  $a = e, i, r, s, d_1, d_2, p_1, p_2, \zeta$  represent nine different neural populations.  $Q_a^{max}$  is the maximum firing rate,  $\theta_a$  is the mean threshold potential, and  $\sigma$  is the standard deviation of firing thresholds. When the membrane potential  $V_a$  exceeds the threshold potential  $\theta_a$ , the neural population will fire with the average firing rate  $Q_a$ .

The variation of the average cell body voltage of the nuclear “ $a$ ” is described by the following equation (Albada et al. 2009; Albada and Robinson 2009b),

$$D_{\alpha\beta}V_a(t) = \sum_{b \in A} S(v_{ab}) \cdot v_{ab} \cdot \phi_b(t) \quad (3)$$

$$D_{\alpha\beta} = \frac{1}{\alpha\beta} \left[ \frac{\partial^2}{\partial t^2} + (\alpha + \beta) \frac{\partial}{\partial t} + \alpha\beta \right] \quad (4)$$

where the differential operator  $D_{\alpha\beta}$  is the dendritic and synaptic integration of the incoming signal.  $\alpha$  and  $\beta$  represent the decay and rise rate of the cell-body potential, respectively.  $v_{ab}$  is the coupling strength value from the neural population of type “ $b$ ” to type “ $a$ ”.  $A$  is a set of populations projecting to the population “ $a$ ”.  $S(v_{ab})$  represents a positive or negative signal. Specifically, if the projection from “ $b$ ” to “ $a$ ” is excitatory, then  $S(v_{ab}) = 1$ ; otherwise,  $S(v_{ab}) = -1$ .  $\phi_b(t)$  is the output pulse rate from the neural population of type “ $b$ ”. For the sake of simplicity, we do not consider the delay of signal transmission between nerve nuclei. However, the receptor  $GABA_B$  acts via second messenger process, we introduce a time delay parameter  $\tau$  on the pathway “ $TRN \rightarrow SRN$ ” to depict its slow dynamics. Therefore, we need a delay differential equation to describe the signal transfer from TRN to SRN (Hu et al. 2015; Hu and Wang 2015; Albada et al. 2009; Albada and Robinson 2009b). Note that the delay is not the main factors to consider in the paper, in addition to special instructions, we all set  $\tau = 0.05$  s.

Finally, the propagation effect of field  $\phi_a$  to other populations is described by a damped wave equation, the speed of propagation is  $v_a$  (Albada et al. 2009; Albada and Robinson 2009b),

$$\frac{1}{\gamma_a^2} \left[ \frac{\partial^2}{\partial t^2} + 2\gamma_a \frac{\partial}{\partial t} + \gamma_a^2 \right] \phi_a(t) = Q_a(t) \quad (5)$$

where  $\gamma_a = v_a/r_a$  is the damping rate, and  $r_a$  is the characteristic axonal range. In fact, all axons of populations except the excitatory pyramidal neurons are too short to support the pulse propagation, it is indicated that  $\phi_c = F(V_c)(c = i, r, s, d_1, d_2, p_1, p_2, \zeta)$  (Hu et al. 2015; Hu and Wang 2015; Albada et al. 2009; Albada and Robinson 2009b). Thus, we only use a damped microwave equation with a source term  $Q_e(t)$  to simulate the transmission effect of the signal on the cortical surface due to the remote excitatory connection (Hu et al. 2015; Hu and Wang 2015; Albada et al. 2009; Albada and Robinson 2009b),

$$\frac{1}{\gamma_e^2} \left[ \frac{\partial^2}{\partial t^2} + 2\gamma_e \frac{\partial}{\partial t} + \gamma_e^2 \right] \phi_e(t) = Q_e(t) \quad (6)$$

Because the connections within the cortex are proportional to the number of synapses involved, similar to previous studies (Hu et al. 2015; Hu and Wang 2015; Albada et al. 2009; Albada and Robinson 2009b), here, we can also further simplify our model, i.e., set  $V_i = V_e$  and  $Q_i = Q_e$ .

Finally, in order to facilitate the numerical calculation, we rewrite the above Eqs. (1)–(5) in the first-order form to describe the BGCT model,

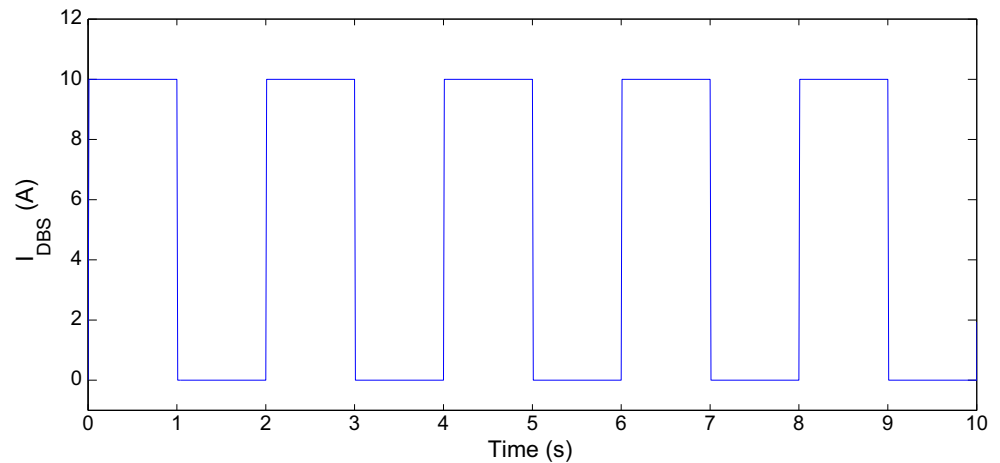
$$\begin{aligned} \frac{d\phi_e(t)}{dt} &= \dot{\phi}_e(t) \\ \frac{d\dot{\phi}_e(t)}{dt} &= \gamma_e^2[-\phi_e(t) + F(V_e(t))] - 2\gamma_e\dot{\phi}_e(t) \\ \frac{dX(t)}{dt} &= \dot{X}(t) \\ X(t) &= [V_e(t), V_{d_1}(t), V_{d_2}(t), V_{p_1}(t), V_{p_2}(t), V_\zeta(t), \\ &\quad V_r(t), V_s(t)]^T \\ \frac{d\dot{V}_e(t)}{dt} &= \alpha\beta(v_{ee}\phi_e + v_{ei}F(V_e) + v_{es}F(V_s) - V_e(t)) \\ &\quad - (\alpha + \beta)\dot{V}_e(t) \\ \frac{d\dot{V}_{d_1}(t)}{dt} &= \alpha\beta(v_{d_1e}\phi_e + v_{d_1d_1}F(V_{d_1}) + v_{d_1s}F(V_s) - V_{d_1}(t)) \\ &\quad - (\alpha + \beta)\dot{V}_{d_1}(t) \\ \frac{d\dot{V}_{d_2}(t)}{dt} &= \alpha\beta(v_{d_2e}\phi_e + v_{d_2d_2}F(V_{d_2}) + v_{d_2s}F(V_s) - V_{d_2}(t)) \\ &\quad - (\alpha + \beta)\dot{V}_{d_2}(t) \\ \frac{d\dot{V}_{p_1}(t)}{dt} &= \alpha\beta(v_{p_1d_1}F(V_{d_1}) + v_{p_1p_2}F(V_{p_2}) + v_{p_1\zeta}F(V_\zeta) \\ &\quad - V_{p_1}(t)) - (\alpha + \beta)\dot{V}_{p_1}(t) \\ \frac{d\dot{V}_{p_2}(t)}{dt} &= \alpha\beta(v_{p_2d_2}F(V_{d_2}) + v_{p_2p_2}F(V_{p_2}) + v_{p_2\zeta}F(V_\zeta) \\ &\quad - V_{p_2}(t)) - (\alpha + \beta)\dot{V}_{p_2}(t) \\ \frac{d\dot{V}_\zeta(t)}{dt} &= \alpha\beta(v_{\zeta e}\phi_e + v_{\zeta p_2}F(V_{p_2}) - V_\zeta(t)) - (\alpha + \beta)\dot{V}_\zeta(t) \\ \frac{d\dot{V}_r(t)}{dt} &= \alpha\beta(v_{re}\phi_e + v_{rp_1}F(V_{p_1}) + v_{rs}F(V_s) - V_r(t) \\ &\quad + I_{DBS} * R) - (\alpha + \beta)\dot{V}_r(t) \\ \frac{d\dot{V}_s(t)}{dt} &= \alpha\beta(v_{se}\phi_e + v_{sp_1}F(V_{p_1}) + v_{sr}^A F(V_r) \\ &\quad + v_{sr}^B F(V_r(T - \tau)) - V_s(t) + \phi_n) - (\alpha + \beta)\dot{V}_s(t) \end{aligned}$$

where the parameter  $\phi_n$  denotes the constant nonspecific subthalamic input onto SRN. Unless otherwise noted, all the parameter values used for the numerical calculation listed in “Appendix”. These values are all derived from real physiological experiments, which appeared in many previous studies.

## Numerical simulation method

All simulations are carried out in the MATLAB environment, and the dynamic equations are solved by the standard four order Runge–Kutta method. We should also illustrate that the step size employed in numerical

**Fig. 2** A specific example of the square wave current used in this paper. Here, we set the period  $P = 2$  s, the amplitude of current  $A = 10$  A, the duration of effective input in one period  $D = 1$  s



calculations is 0.00005 s, which is small enough to verify exact solutions of the equation. In all simulations, we used a random initial condition at each parameter point. Firstly, we study the transfer behavior between different states by using the bifurcation analysis method over the inhibitory coupling strength parameter  $-v_{sr}$  on the pathway “ $TRN \rightarrow SRN$ ” (Fig. 3a). The bifurcation diagram is obtained by taking the local maximum and minimum values of cortical excitatory axon field ( $\phi_e$ ) over changing of  $-v_{sr}$ , the unstable transient of the system is removed during the simulation. Similarly, we can obtain the different shock states bifurcation diagram of the system in the two-dimensional parameter plane. For example, Figs. 5, 6 and 7 are obtained by setting 31 points in the interval  $[0.1, 2]$  for period  $P$ , which show the interesting bidirectional periodic adjustment phenomenon. If we increase number of points in  $[0.1, 2]$  for  $P$ , similar periodic phenomena would also appear in the bifurcation diagram. Finally, we used the power spectrum of time series  $\phi_e(t)$  to analyze the dominant frequency of the nuclear oscillation (such as, Fig. 5b). The study result shows that the frequency of EPN shock mainly fall in the range of 2–4 Hz, which is the typical frequency range of absence epilepsy. In order to better understand the control mechanism of seizures, in some places, we simulated the average discharge rates (MFRs) of several critical populations (such as, Fig. 7d). In this paper, we suppose that the seizure induced by the inhibitory coupling strength of the pathway “ $TRN \rightarrow SRN$ ”.

### The onset mechanism of the absence seizure induced by $-v_{sr}$

Figure 3a is the transition diagram between different states of the brain with varying of  $-v_{sr}$ . As increasing of  $-v_{sr}$ , there are four states appeared in EPN successively: (1) the saturation state; (2) the seizure state; (3) the simple oscillation state; (4) the low frequency discharge state. Figure 3b–e are four specific oscillation time sequence diagrams obtained by setting  $-v_{sr} = 0.38$  mV s,  $-v_{sr} = 1.2$  mV s,  $-v_{sr} = 1.58$  mV s and  $-v_{sr} = 2.0$  mV s, respectively. The saturation state (1) refers to the brain concussion with the frequency of 250 Hz (i.e.,  $Q_e^{max}$ ), it is an ideal state, usually only seen in theoretic study. The state of epileptic seizure (2) is a periodic oscillation, oscillation frequencies appear four extreme points in one period. The simple oscillation state (3) is a kind of periodic oscillation, similar to sine wave, it is usually represented a transitional state between the normal state and seizures, caused by Hopf bifurcation. The low frequency discharge state (4) refers to the brain concussion phenomenon with low frequency, it represents the normal state of the brain.

This transfer mechanism is easily explained in Fig. 1.  $-v_{sr}$  is the inhibitory coupling strength on the pathway “ $TRN \rightarrow SRN$ ”, increasing of  $-v_{sr}$  can lead to the decreased activation level of SRN, thus the excitatory output from SRN to EPN will also be reduced, finally, the activation level of EPN decreased. Therefore, with the increase of  $-v_{sr}$ , the discharge activity level of EPN

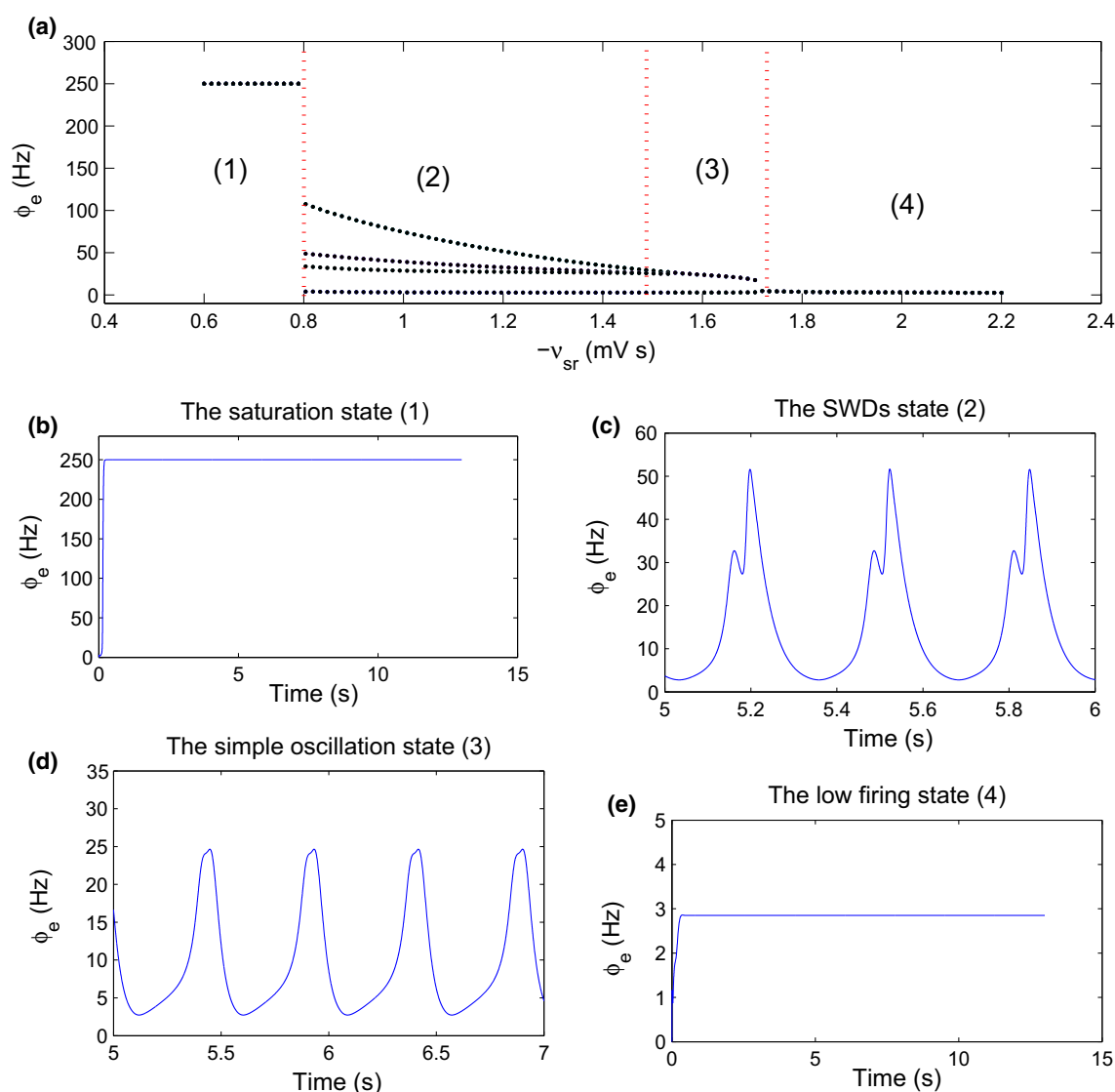


**Fig. 3** **a** The transition diagram between different states (1)–(4) of the brain with varying of  $-v_{sr}$ . With increasing of  $-v_{sr}$ , the state (1), (2), (3) and (4) appeared successively. We set  $\tau = 0.065$  s,  $v_{ee} = 1.2$  mV s,  $v_{rs} = 0.55$  mV s,  $v_{es} = 2$  mV s,  $v_{se} = 2.3$  mV s,  $v_{\zeta e} = 0.15$  mV s and  $v_{p_1\zeta} = 0.1$  mV s in simulations. **b–e** Four

specific oscillation time sequence diagrams obtained by setting  $-v_{sr} = 0.38$  mV s,  $-v_{sr} = 1.2$  mV s,  $-v_{sr} = 1.58$  mV s and  $-v_{sr} = 2.0$  mV s in (a), respectively

gradually decreased, four states (1)–(4) appeared successively. In order to better understand this mechanism, we simulate the MFRs of EPN in Fig. 4. In Fig. 4, we find that the average oscillation frequency of EPN decreases gradually, as increasing of  $-v_{sr}$ , which agrees with the above analysis.

## Main results

In this section, we employ the deep brain stimulation voltage on STN to study the effect of the period P and duration D of current stimulation on the epileptic seizure.

## Control seizures by changing the period of stimulation current

Seizures are mainly produced in the thalamocortical network, SNr is the major output nucleus from the basal ganglia to the thalamus. Based on anatomical structure and function, the thalamus can be divided into the thalamic reticular nucleus and thalamic relay nuclei, and the relative connection strength between the pathway “SNr  $\rightarrow$  TRN” and the pathway “SNr  $\rightarrow$  SRN” is uncertain (Chen et al. 2014, 2015; Hu et al. 2015; Hu and Wang 2015; Hu et al. 2017; Albada et al. 2009; Albada and Robinson 2009b; Shimo et al. 2014). The pathway “SNr  $\rightarrow$  TRN” is often

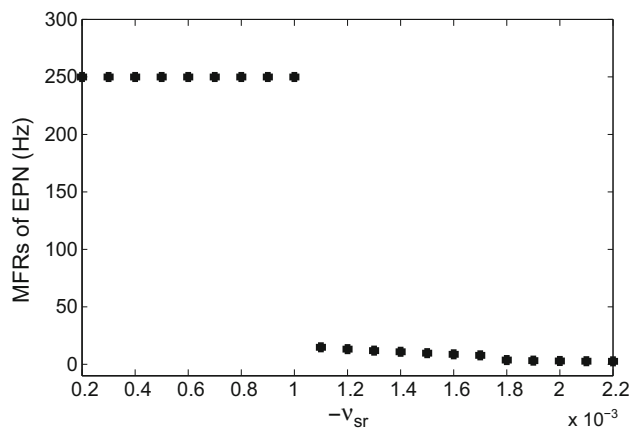


**Fig. 4** The average oscillation frequency (MFRs) of EPN with changing of  $-v_{sr}$ . With increasing of  $-v_{sr}$ , MFRs decreased gradually, which agrees with the bifurcation trend in Fig. 3a

neglected in theoretical model studies of other neurological diseases, such as Parkinson's disease (Albada et al. 2009; Albada and Robinson 2009b).

For a more comprehensive study on anatomical structure of the brain, in this paper, we consider together the effect of the pathway " $SNr \rightarrow TRN$ " and pathway " $SNr \rightarrow SRN$ " on seizures. Firstly, we assume that there is no connection from SNr to TRN, i.e.,  $v_{pp1} = 0$  mV s, only considering the control effect of the pathway " $SNr \rightarrow SRN$ ". We study the control effect on the two-dimensional parametric plane  $(-v_{sr}, P)$ . Figure 5a shows the bifurcation diagram of the states. Four different states appeared on EPN as increasing of  $-v_{sr}$ . Seizure activity can be effectively controlled by turning the period P into some suitable intervals, indicated by bidirectional arrows (marked in the attack intervals) in Fig. 5a. It is an interesting bidirectional periodic alternating phenomenon. Figure 5b is the dominant frequency analysis diagram corresponding to Fig. 5a. In Fig. 5b, we clearly see that the frequency of seizures in the model mainly falls within the range of 2–4 Hz, which is the typical absence seizures status. Figure 5c is a specific state bifurcation diagram obtained by setting  $-v_{sr} = 0.6$  mV s in Fig. 5a, it is shown the apparent transition phenomenon between SWDs oscillation and low frequency oscillation. Figure 5d is the variation trend of MFRs of EPN with increasing of P, obtained by setting  $-v_{sr} = 0.6$  mV s, which compares well with Fig. 5c. We think the DBS will ultimately affect the firing activation level of EPN, so the Fig. 5d may help us to better understand the control mechanism.

Secondly, we assume that  $v_{sp1} = 0$  mV s, to study the control effect of the single pathway " $SNr \rightarrow TRN$ " on seizures. Figure 6a is the corresponding state region bifurcation diagram. The model appearing four different

states (1)–(4) with varying of  $-v_{sr}$ . Seizures can also be controlled by turning P into some appropriate intervals, indicated by bidirectional arrows in Fig. 6a. Figure 6b is the dominant frequency analysis diagram. Figure 6c, d are two typical state bifurcation diagrams obtained by setting  $-v_{sr} = 0.85$  mV s and  $-v_{sr} = 1.5$  mV s in Fig. 6a, respectively. Figure 6c shows that the seizure controlled through the transition to the saturated state; Fig. 6d implies that the seizure also may be inhibited through transferring with the low frequency oscillatory state. Figure 6e is the MFRs of EPN obtained by setting the same parameter with Fig. 6d. MFRs level appears periodic alternation, the trend fits with the bifurcation situation in Fig. 6d.

Finally, we suppose that SNr has outputs both to TRN and SRN. In this case, we set  $v_{sp1} = 0.035$  mV s and  $v_{pp1} = 0.035$  mV s, they are both within the reasonable range of biology significance. Figure 7a is the state regional bifurcation diagram. There are four different states appeared in EPN with varying of parameters. If we adjust the period P to appropriate values, denoted by bidirectional arrows in Fig. 7a, the seizure state (2) can be well controlled. The corresponding dominant frequency analysis is shown in Fig. 7b. A specific bifurcation diagram of  $\phi_e$  over the period P obtained by setting  $-v_{sr} = 1.2$  mV s in Fig. 7a. It can be observed from Fig. 7c that there is an obvious shift between the epileptic seizure state and the simple oscillation state. Fig. 7d is the MFRs of EPN, SNr, STN, SRN and TRN, respectively. It is shown that the overall change trend of MFRs for these critical populations is consistent with the bifurcation diagram in Fig. 7c.

### Control seizures by changing the duration D of stimulation current in one period

Similar to the study of "Control seizures by changing the period of stimulation current" section, here, we also fully consider the connection between SNr and thalamus. The following research is divided into three parts, and we consider the control effect in the plane  $(-v_{sr}, D)$ .

First of all, we suppose that  $v_{pp1} = 0$  mV s. Figure 8a is the bifurcation diagram of four states. We can see from the arrows in Fig. 8a that if the parameter D falls into appropriate intervals, the seizure can be well controlled via transferring to the low frequency oscillation state. Figure 8b is the corresponding frequency analysis results. Figure 8c is a typical bifurcation diagram obtained by letting  $-v_{sr} = 0.6$  mV s in Fig. 8a. It shows the obvious transfer behavior between the epileptic oscillation state and the low frequency firing state. Figure 8d is the MFRs of EPN with the change of D, obtained by setting the same parameters as in Fig. 8c. The MFRs trend are also periodic,

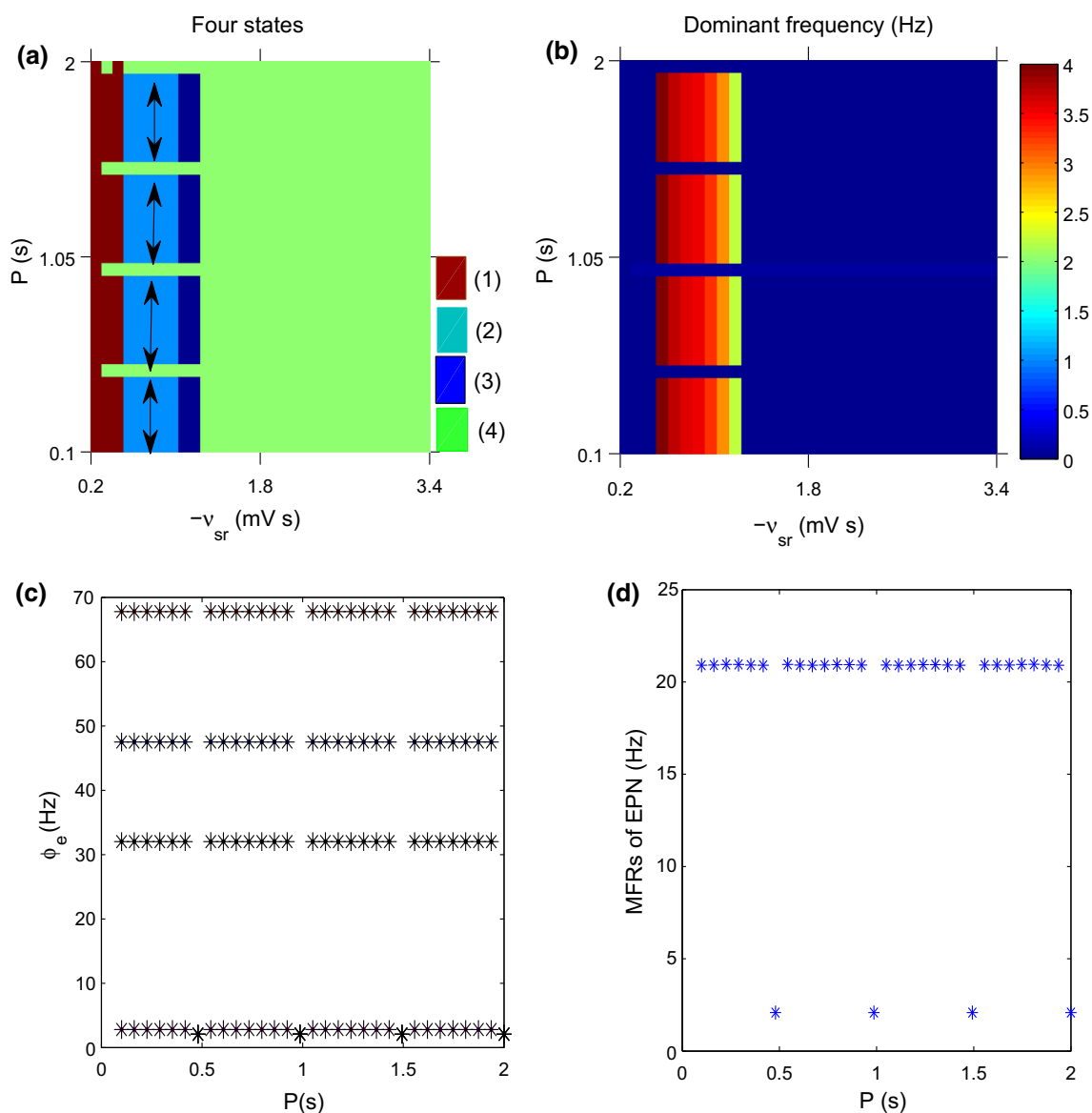


**Fig. 5** **a, b** The state transitions and dominative frequency analysis in the parameter plane ( $-v_{sr}, P$ ). Here, we assume that there is no connection from SNr to TRN, i.e.,  $v_{tp1} = 0$  mV s; and  $A = 50$  A,  $D = 0.0006$  s,  $v_{p1\zeta} = 0.1$  mV s. Four different states are shown by different colors. It is shown that the states of absence seizure can be controlled by tuning  $P$  into some reasonable intervals, indicated by

and qualitative fitting with the state bifurcation situation in Fig. 8c.

Secondly, we assume that the coupling strength  $v_{sp1} = 0$  mV s. In this case, when the  $D$  is adjusted to some reasonable intervals, the seizure activity can also be controlled, shown in Fig. 9a. We give the corresponding frequency analysis results in Fig. 9b. It shows that the seizure frequency is main in the range of 2–4 Hz. A specific bifurcation diagram of  $\phi_e$  as the function of  $D$  is obtained by setting  $-v_{sr} = 1.32$  mV s in Fig. 9c, which shows the transition process between the epileptic oscillation state

the arrows. In (b), we can clear see that the frequency of seizures caused by this model mainly falls within the range of 2–4 Hz, which is the typical absence seizures status. **c** A specific bifurcation diagram of  $\phi_e$  obtained by setting  $-v_{sr} = 0.6$  mV s in (a). **d** The MFRs of EPN with increasing of  $P$ , obtained by setting  $-v_{sr} = 0.6$  mV s, which compares well with (c). (Color figure online)

and the simple oscillation state. Figure 9d describes the variation trend of MFRs, obtained by setting  $-v_{sr} = 1.32$  mV s, where, the relative low MFRs represent the simple oscillation state and another is the seizure state. These two levels of MFRs alternate occurrence with increasing of  $D$ .

Finally, we set  $v_{sp1} = 0.035$  mV s and  $v_{tp1} = 0.035$  mV s, respectively. Figure 10a is the state regional bifurcation diagram in the plane ( $-v_{sr}, D$ ) in this case. There are four different states appeared in EPN with changing of  $-v_{sr}$ . If we control the duration  $D$  to some

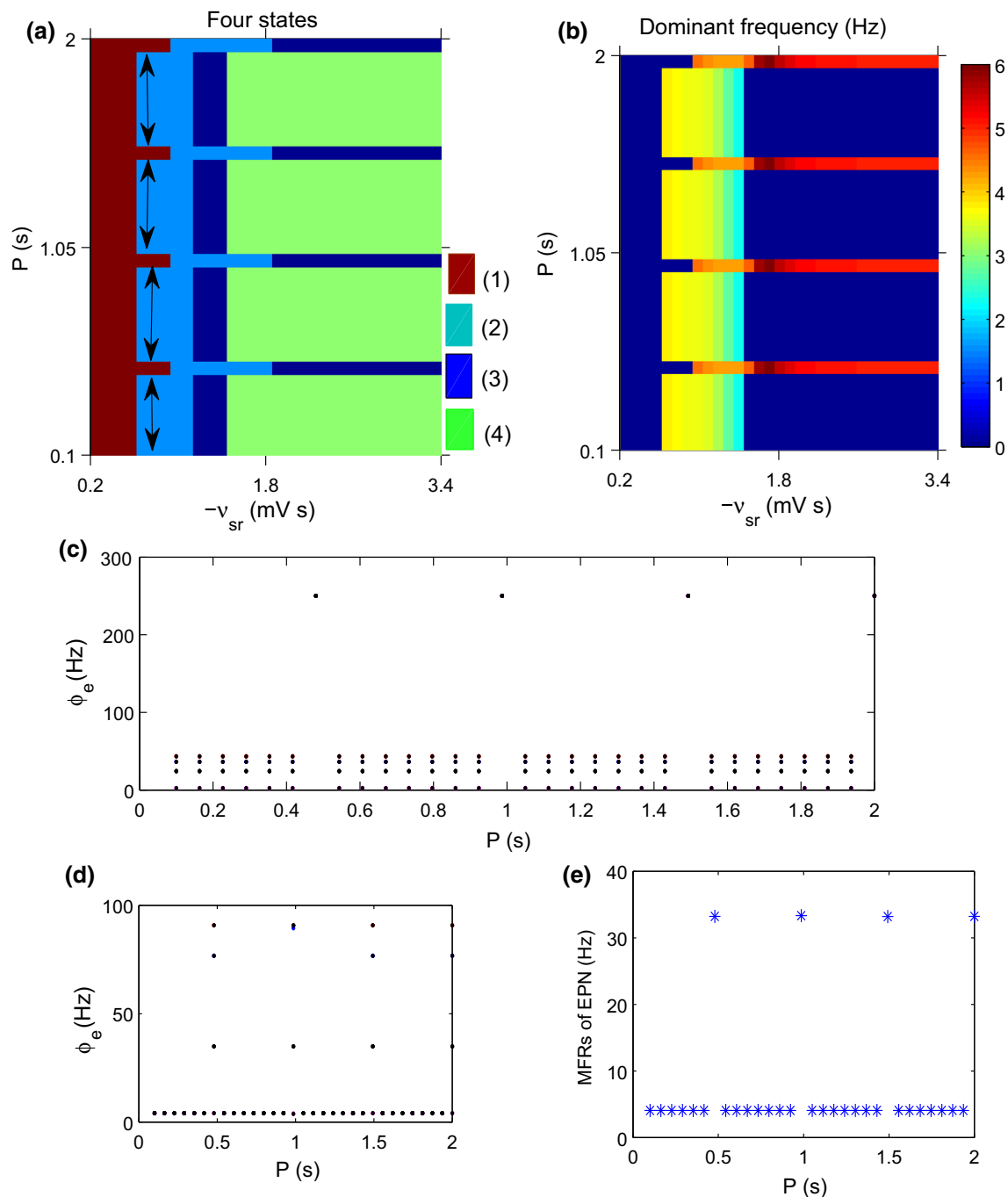


**Fig. 6** **a, b** The state transitions and dominative frequency analysis in the parameter plane  $(-v_{sr}, P)$ . Here, we assume that there is no connection from SNr to SRN, i.e.,  $v_{sp_i} = 0$  mV s; and  $A = 50$  A,  $D = 0.0006$  s,  $v_{p_i\zeta} = 0.1$  mV s. Four different states are shown by different colors. It is shown that the seizure state can be controlled by tuning  $P$  into some reasonable intervals, indicated by the arrows. In **(b)**, we can clear see that the frequency of seizures mainly falls within

the range of 2–4 Hz, which is the typical absence seizures status. **c, d** Two typical state bifurcation diagrams obtained by setting  $-v_{sr} = 0.85$  mV s and  $-v_{sr} = 1.5$  mV s in **(a)**, respectively. **e** The MFRs of EPN obtained by setting the same parameter with **(d)**. MFRs level also appears periodic alternation, the tread fits with the bifurcation situation in **(d)**. (Color figure online)

appropriate ranges, indicated by bidirectional arrows in Fig. 10a, the seizure state (2) can be pushed into the low frequency oscillation state (4). The dominant frequency

analysis is shown in Fig. 10b. A specific bifurcation diagram of  $\phi_e$  over  $D$  obtained by setting  $-v_{sr} = 1.7$  mV s in Fig. 10a. It can be observed from Fig. 10c that there exists

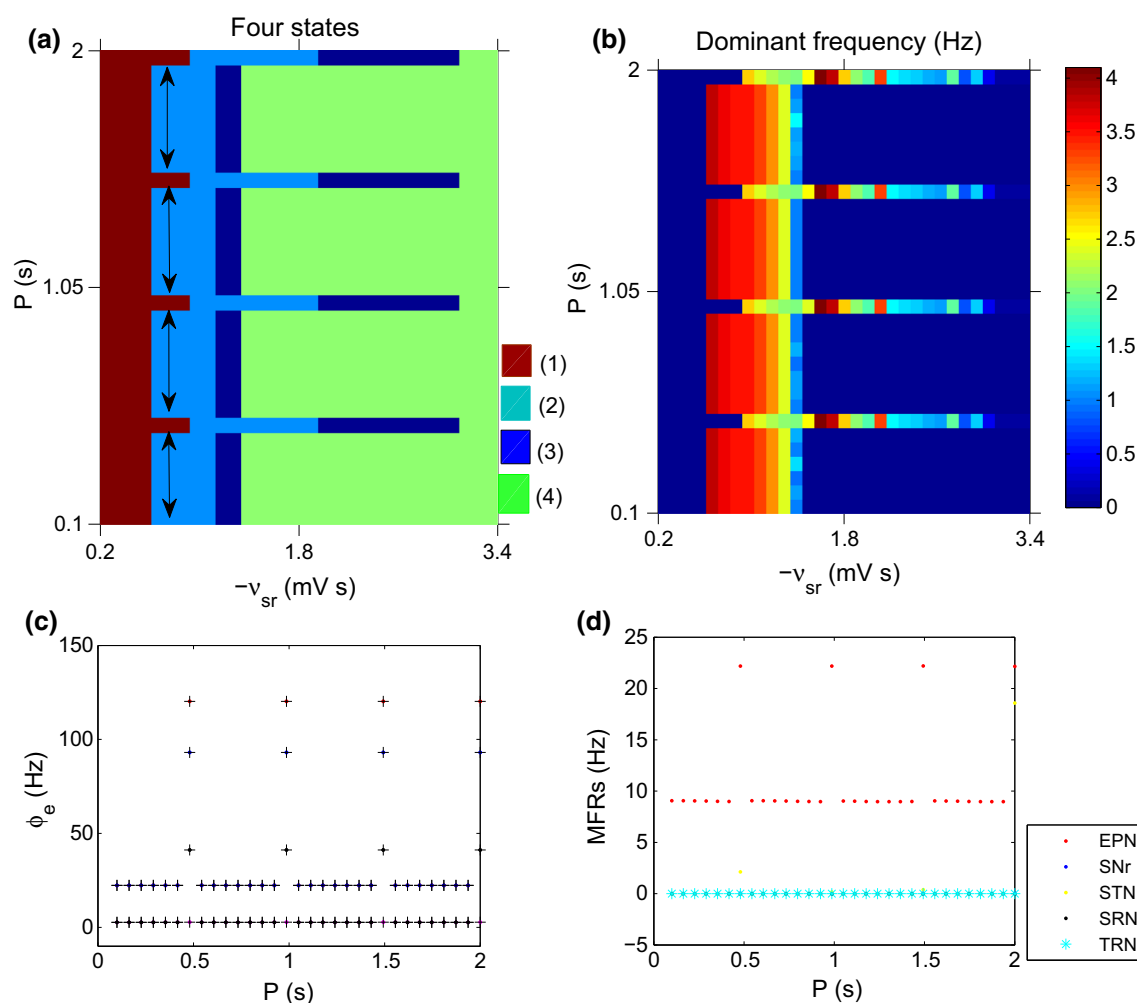


**Fig. 7** **a, b** The state transitions and dominant frequency analysis diagram in the panel  $(-v_{sr}, P)$ . In this case, we assume that SNr has outputs both to TRN and SRN. We set  $v_{sp1} = 0.035$  mV s;  $v_{rp1} = 0.035$  mV s;  $A = 50$  A;  $D = 0.0006$  s;  $v_{p1}\zeta = 0.1$  mV s. Four different states are distinguished by different colors. Indicated by the double arrows, we know that the seizure can be controlled by tuning the period  $P$ . In **(b)**, we can easily see that the frequency of these

seizures on EPN mainly fall into the range of 2–4 Hz, which is the typical absence seizure frequency. **c** A specific bifurcation diagram of  $\phi_e$  obtained by setting  $-v_{sr} = 1.2$  mV s in **(a)**. **d** The MFRs of the EPN, SNr, STN, SRN and TRN, respectively. It is shown that the overall change trend of MFRs for these critical populations is consistent with the bifurcation diagram **(c)**. (Color figure online)

an obvious shift between the epileptic seizure state and the low frequency oscillation state.

Figure 11a is a MFRs diagram for EPN, corresponding to Fig. 10c. It is shown that the high and low oscillating frequency appeared alternately, corresponding to the transition process between the epileptic oscillation state and the low frequency oscillation state. Figure 11b simulates the MFRs of the EPN, SNr, STN, SRN and TRN, respectively. It is shown that the overall trend of MFRs for these critical populations is consistent with Fig. 11a and the bifurcation diagram Fig. 10c. We know that the state of the EPN ultimately depends on the MFRs of itself and other critical nerve nuclei, so, we hope that the Fig. 11 might further help us to understand the control mechanism of this model.

## Conclusion

Epilepsy is a kind of chronic disease, it will last for years, even decades, and has serious negative impact on patient's physical, mental, marital and social economy, etc. Therefore, we should pay enough attention to the treatment of patients with epilepsy. Control is the most important strategy in the treatment of epilepsy. In this paper, based on a theoretical model, we changed the period and duration of stimulation current to study the control mechanisms of absence seizures. We can see from the numerical simulation results that seizures can be controlled effectively by turning the period and duration of current stimulation into suitable ranges. It is a very interesting bidirectional

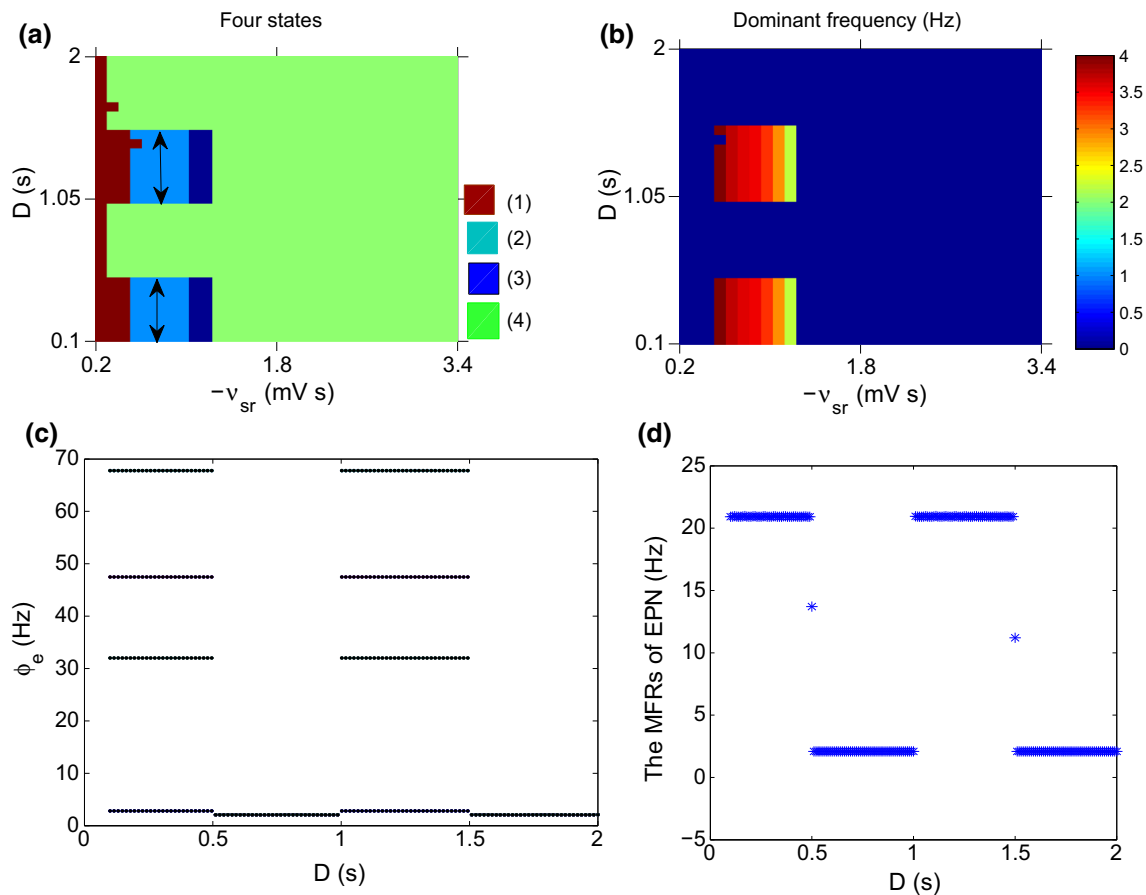


**Fig. 8** **a, b** The state bifurcation and dominant frequency analysis results in the parameter panel ( $-v_{sr}, D$ ). Here, we suppose that there is no projection from SNr to TRN, i.e., let  $v_{p1} = 0$  mV s; and set  $A = 50$  A,  $T = 1$  s,  $v_{p1\zeta} = 0.1$  mV s. Four states are represented by different colors. It is shown that the state of seizures may be

controlled by tuning  $D$  into suitable intervals, shown by the arrows. In **(b)**, we can observe that the frequency of seizures mainly falls in the range of 2–4 Hz. **c** A specific bifurcation diagram of  $\phi_e$  obtained by setting  $-v_{sr} = 0.6$  mV s in **(a)**. **d** The average oscillation frequency of EPN with the change of  $D$  corresponds to **(c)**. (Color figure online)

periodic adjustment phenomenon. However, the control effect is not obvious by changing the magnitude of the current. Of course, this program is also little used in clinical medicine and experimental research at present. The target chosen is the STN, which is also the most commonly used deep brain stimulation target area in clinical medicine. The current parameters  $P$  and  $D$  studied in this paper may be easily regulated by the high tech clinical experiment technology, therefore, we hope that the obtained results can provide a valuable theoretical reference for clinical and experimental research in future.

Of course, in addition to the STN, many of recent studies have shown that the deep brain stimulation acted on the thalamus (Hu et al. 2017; Lehtimäki et al. 2016; Krishna et al. 2016), SNr (Chen et al. 2014; Guo et al.

2014; Hu et al. 2015; Hu and Wang 2015), Gpe (Chen et al. 2015), striatum (Hu et al. 2017), etc., also have well therapeutic effect. In addition to the typical square wave current used in this paper, there are also other common employed current types, such as, the triangle function wave, the triangle wave, the coordinated reset current stimulation, etc., have been proved that may have good effects on the control of epilepsy in clinical trials. Therefore, the future theoretical research should focus on selecting of the optimal stimulus target area and stimulus programme. On the other hand, as introduced in the section of Introduction, seizures are mainly caused by abnormal interactions between the cortical and thalamic networks. Besides the coupling weight  $-v_{sr}$  (Fig. 3), many other critical factors in the network, such as the

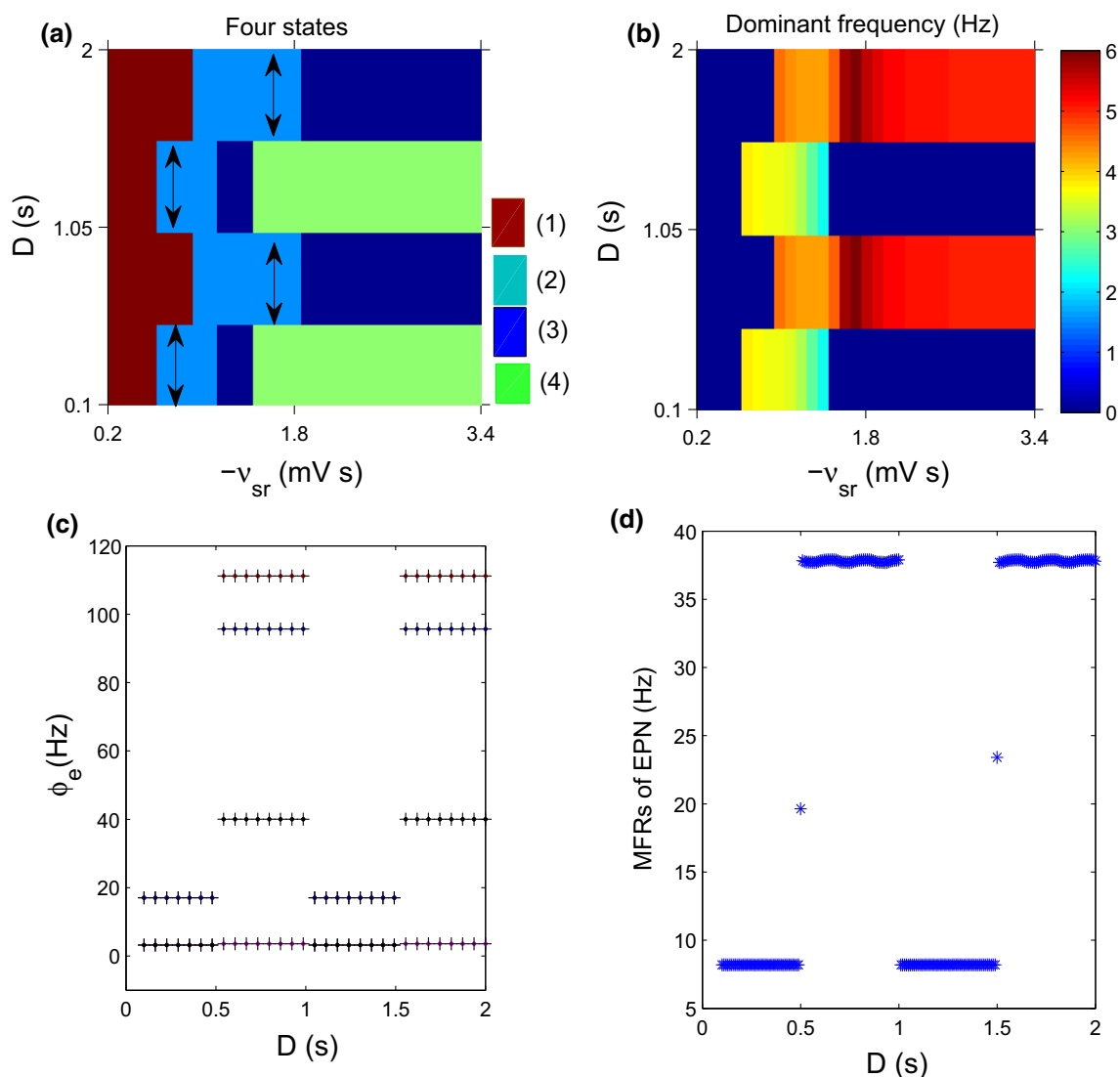


**Fig. 9** **a, b** The state transitions and dominative frequency analysis results in the parameter plane ( $-v_{sr}$ ,  $D$ ). Here, we consider the single control effect of the pathway “ $SNr \rightarrow TRN$ ”, and set  $v_{sp1} = 0$  mV s;  $A = 50$  A;  $T = 1$  s;  $v_{p1\zeta} = 0.1$  mV s. Four different states (1)–(4) are shown by different colors. It is shown that the state of absence seizures can be controlled by tuning  $D$  into some reasonable intervals. In **(b)**, we can see that the frequency of seizures mainly falls within

the range of 2–4 Hz, which is the typical absence seizures status. **c** A typical state bifurcation diagram obtained by setting  $-v_{sr} = 1.32$  mV s in **(a)**. **d** The variation trend of MFRs obtained by setting  $-v_{sr} = 1.32$  mV s, where, the relative low MFRs represent the simple oscillation state and another is the seizure state. (Color figure online)

delay (Breakspear et al. 2006; Marten et al. 2009a, b; Chen et al. 2014), some excitatory pathways related to SRN (Hu et al. 2015), etc., can also induce epilepsy. We think that the method employed in the model can be generalized to these situations, and can obtain similar control effects.

At last, we should point out some limits of the model and method as follows, (1) all results are not observed directly in the experiment by now. Therefore, there still needs

relative experiments to verify the rationality of them. Especially, the effective control intervals shown in Figs. 5, 6 and 7 are very narrow, whether these cases easily realized in clinical experiments are still need to be verified. On the other hand, the real brain environment is very complex for each patient, whether the effective control band for  $P$  and  $D$  can be easily found for different patients is still needed to be verified in future research. And, the scan and assessment of the control effect in the parameter plane ( $P, D$ )

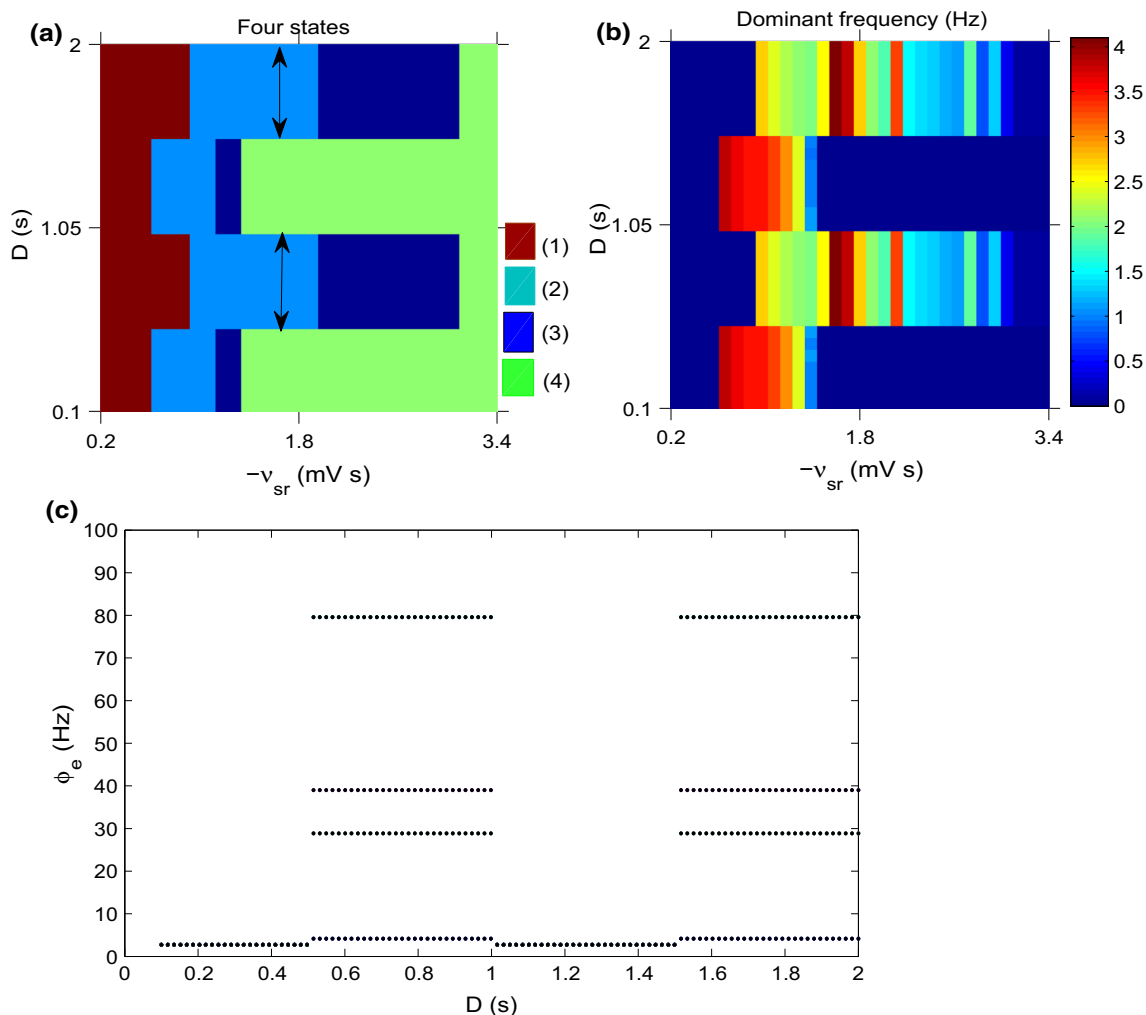


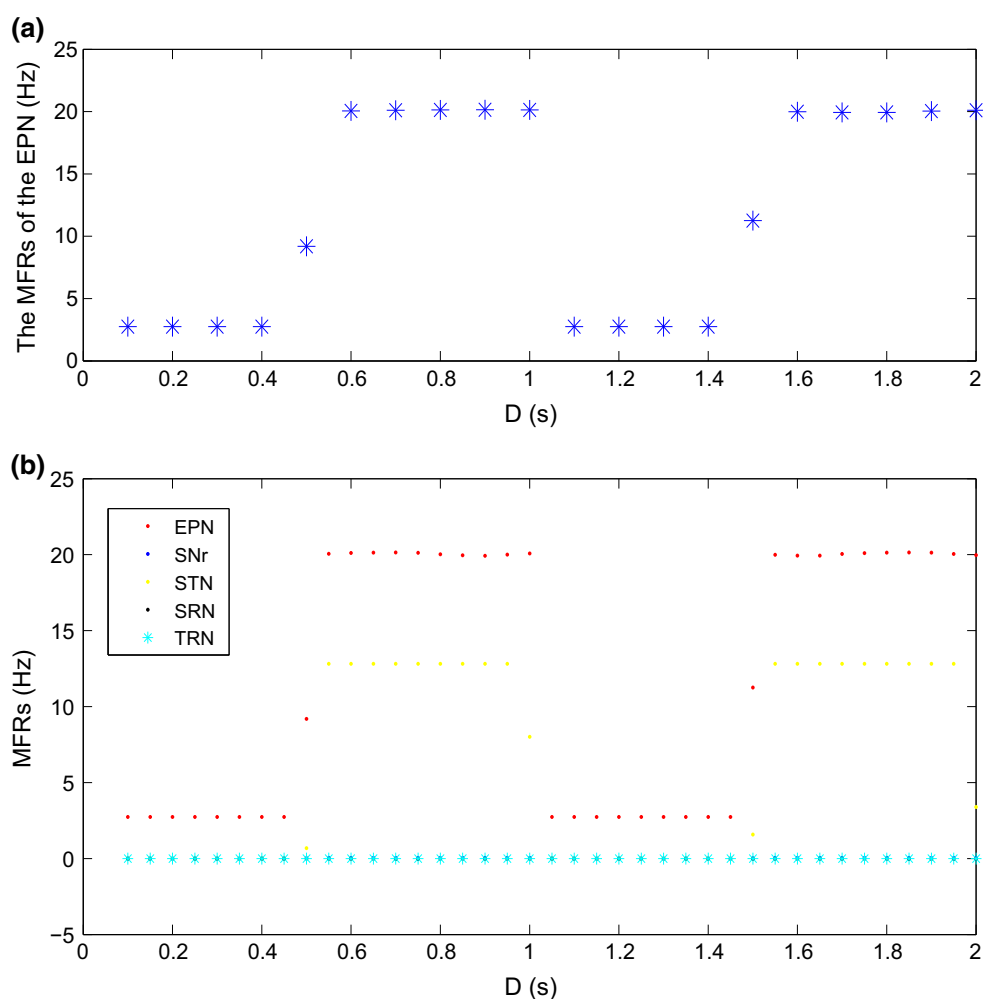
**Fig. 10** **a, b** The state transitions and dominative frequency analysis in the parameter plane  $(-v_{sr}, D)$ . Here, we assume that SNr has outputs both to TRN and SRN. In this case, we set  $v_{sp1} = 0.035$  mV s and  $v_{p1} = 0.035$  mV s; and  $A = 50$  A,  $T = 1$  s,  $v_{p1}\zeta = 0.1$  mV s. Four different states are shown by different colors. It is shown that the states of absence seizure can be controlled by tuning  $D$  into some

reasonable intervals, indicated by the arrows. In **(b)**, we can clear see that the frequency of seizures caused by this model mainly falls within the range of 2–4 Hz, which is the typical absence seizures status. **c** A specific bifurcation diagram of  $\phi_e$  obtained by setting  $-v_{sr} = 1.7$  mV s in **(a)**, which shows that the obvious transition process between the state (2) and (4). (Color figure online)

may shed more light onto the reliability of our results. (2) We should also admit that the highest stimulation frequency employed in our simulations is 10 Hz, which is not a traditional DBS frequency, and whether higher stimulation frequencies have similar effects is still needed to be verified in future. (3) The type of epilepsy shown in this model is the absence seizure. However, absence seizure may be easily controlled by drugs shown in some previous studies. The DBS as an “invasive treatment” method, whether it is suitable for the absence seizure, or where is his advantage compared to the drug method is still unclear, need to be considered further. (4) The mean field model is a simplified idealized model, although it is easy to realize in the calculation, at the same time, it also omits many important

physiological parameters of the brain, such as, the concentration of ion channels, the connection structure between neurons, etc., should be considered resorting to the spike model in our future work. (5) Although the MFRs diagram can help us to understand the control mechanism, we found that the exact understanding on these is still difficult based on this model. (6) We should also notice that the “control” effect mentioned in the paper means the transition process between the seizure state (2) and three other states, rather than the transition from the epileptic seizure to the normal state. Because what the meaning of the state (1), (3) and (4) should be verified by the experiment, such as the saturated state (1) may represent an excessive firing activity even beyond that of epilepsy seizures.

**Fig. 11 a** The MFRs of EPN with changing of  $D$  corresponds to Fig. 10c, here, we set  $-v_{sr} = 1.7$  mV s. **b** The MFRs of the EPN, SNr, STN and TRN, respectively. It is shown that the overall change trend of MFRs for these critical populations is consistent with (a) and the bifurcation diagram Fig. 10c, which may further help us to understand the control mechanism of this model



**Acknowledgements** This research was supported by the National Science Foundation of China (Grant No. 11602092); The Fundamental Research Funds for the Central Universities (Grant No. 2662015QD040) and The National Undergraduate Training Program for Innovation and Entrepreneurship of Huazhong Agricultural University (Grant No. 201710504092).

## Appendix

Unless otherwise noted, we use the following parameter values to numerical simulations (Robinson et al. 2002; Marten et al. 2009a, b; Chen et al. 2014, 2015; Hu et al. 2015; Hu and Wang 2015; Hu et al. 2017; Albada et al. 2009; Albada and Robinson 2009b; Roberts and Robinson 2008; Robinson et al. 1998, 2001, 2004; Breakspear et al. 2006,

Parameter	Meaning	Value
$Q_e^{max}, Q_i^{max}$	Cortical maximum firing rate	250 Hz
$Q_{d_1}^{max}, Q_{d_2}^{max}$	Striatum maximum firing rate	65 Hz
$Q_{p_1}^{max}$	SNr maximum firing rate	250 Hz
$Q_{p_2}^{max}$	GPe maximum firing rate	300 Hz
$Q_{\zeta}^{max}$	STN maximum firing rate	500 Hz
$Q_s^{max}$	SRN maximum firing rate	250 Hz
$Q_r^{max}$	TRN maximum firing rate	250 Hz
$\theta_e, \theta_i$	Mean firing threshold of cortical populations	15 mV
$\theta_{d_1}, \theta_{d_2}$	Mean firing threshold of striatum	19 mV
$\theta_{p_1}$	Mean firing threshold of SNr	10 mV
$\theta_{p_2}$	Mean firing threshold of GPe	9 mV
$\theta_{\zeta}$	Mean firing threshold of STN	10 mV
$\theta_s$	Mean firing threshold of SRN	15 mV

Parameter	Meaning	Value
$\theta_r$	Mean firing threshold of TRN	15 mV
$\gamma_e$	Cortical damping rate	100 Hz
$\tau$	Time delay due to slow synaptic kinetics of $GABA_B$	50 ms
$\alpha$	Synaptodendritic decay time constant	$50 \text{ s}^{-1}$
$\beta$	Synaptodendritic rise time constant	$200 \text{ s}^{-1}$
$\sigma$	Threshold variability of firing rate	6 mV
$\phi_n$	Nonspecific subthalamic input onto SRN	2 mV s

Coupling strength	Source	Target	Value
$v_{ee}$	Excitatory pyramidal neurons	Excitatory pyramidal neurons	1 mV s
$v_{ei}$	Inhibitory interneurons	Excitatory pyramidal neurons	- 1.8 mV s
$v_{re}$	Excitatory pyramidal neurons	TRN	0.05 mV s
$v_{rs}$	SRN	TRN	0.5 mV s
$v_{sr}^{A,B}$	TRN	SRN	(- 3.8) to (- 0.2) mV s
$v_{d_1e}$	Excitatory pyramidal neurons	Striatal D1 neurons	1 mV s
$v_{d_1d_1}$	Striatal D1 neurons	Striatal D1 neurons	- 0.2 mV s
$v_{d_1s}$	SRN	Striatal D1 neurons	0.1 mV s
$v_{d_2e}$	Excitatory pyramidal neurons	Striatal D2 neurons	0.7 mV s
$v_{d_2d_2}$	Striatal D2 neurons	Striatal D2 neurons	- 0.3 mV s
$v_{d_2s}$	SRN	Striatal D2 neurons	0.05 mV s
$v_{p_1d_1}$	Striatal D1 neurons	SNr	- 0.1 mV s
$v_{p_1p_2}$	GPe	SNr	- 0.03 mV s
$v_{p_1\zeta}$	STN	SNr	0-0.6 mV s
$v_{p_2d_2}$	Striatal D2 neurons	GPe	- 0.3 mV s
$v_{p_2p_2}$	GPe	GPe	- 0.075 mV s
$v_{p_2\zeta}$	STN	GPe	0.45 mV s
$v_{\zeta p_2}$	GPe	STN	- 0.04 mV s
$v_{es}$	STN	Excitatory pyramidal neurons	1.8 mV s
$v_{se}$	Excitatory pyramidal neurons	SRN	2.2 mV s

Coupling strength	Source	Target	Value
$v_{\zeta e}$	Excitatory pyramidal neurons	STN	0.1 mV s
$v_{sp_1}$	SNr	SRN	- 0.035 mV s
$v_{rp_1}$	SNr	TRN	- 0.035 mV s

## References

Arakaki T, Mahon S, Charpier S, Leblois A, Hansel D (2016) The role of striatal feedforward inhibition in the maintenance of absence seizures. *J Neurosci* 36(37):9618–9632

Breakspear M, Roberts JA, Terry JR, Rodrigues S, Mahant N, Robinson PA (2006) A unifying explanation of primary generalized seizures through nonlinear brain modeling and bifurcation analysis. *Cereb Cortex* 16(9):1296–1313

Case M, Soltesz I (2011) Computational modeling of epilepsy. *Epilepsia* 52(s8):12–15

Chabards S, Kahane P, Minotti L, Koussie A, Hirsch E, Benabid AL (2002) Deep brain stimulation in epilepsy with particular reference to the subthalamic nucleus. *Epileptic Disord* 4(3):83–93

Chambers A, Bowen JM (2013) Electrical stimulation for drug-resistant epilepsy: an evidence-based analysis. *Ont Health Technol Assess Ser* 13(18):1–37

Chen MM, Guo DQ, Wang TB, Jing W, Xia Y, Xu P, Luo C, Valdes-Sosa PA, Yao DZ (2014) Bidirectional control of absence seizures by the basal ganglia: a computational evidence. *PLoS Comput Biol* 10(3):e1003495

Chen MM, Guo DQ, Li M, Ma T, Wu SD, Ma JI, Cui Y, Xia Y, Xu P, Yao DZ (2015) Critical roles of the direct GABAergic pallidocortical pathway in controlling absence seizures. *PLoS Comput Biol* 11(10):e1004539

Child ND, Stead M, Wirrell EC, Nickels KC, Wetjen NM, Lee KH, Klassen BT (2014) Chronic subthreshold subdural cortical stimulation for the treatment of focal epilepsy originating from eloquent cortex. *Epilepsia* 55(3):e18–e21

Coenen AM, Van Luijckelaar EL (2003) Genetic animal models for absence epilepsy: a review of the WAG/Rij strain of rats. *Behav Genet* 33:635–655

Crunelli V, Leresche N (2002) Childhood absence epilepsy: genes, channels, neurons and networks. *Nat Rev Neurosci* 3:371–382

Da Cunha C, Boschen SL, Gomez-a A, Ross EK, Gibson WSJ, Min HK, Lee KH, Blaha CD (2015) Toward sophisticated basal ganglia neuromodulation: review on basal ganglia deep brain stimulation. *Neurosci Biobehav Rev* 58:186–210

Dadok VM, Szeri AJ, Kirsch H, Sleight J, Lopour B (2012) Interpretation of seizure evolution pathways via a mean-field cortical model. *BMC Neurosci* 13(Suppl 1):95

De Hemptinne C, Swann NC, Ostrem JL, Ryapolova-Webb ES, Luciano MS, Galifianakis NB, Starr PA (2015) Therapeutic deep brain stimulation reduces cortical phase-amplitude coupling in Parkinson’s disease. *Nat Neurosci* 18(5):779–786

Deransart C, Depaulis A (2002) The control of seizures by the basal ganglia? A review of experimental data. *Epileptic Disord* 4(3):61–72

Deransart C, Vercueil L, Marescaux C, Depaulis A (1998) The role of basal ganglia in the control of generalized absence seizures. *Epilepsy Res* 32(1):213–223

- Fan DG, Wang QY, Perc M (2015) Disinhibition-induced transitions between absence and tonic-clonic epileptic seizures. *Sci Rep* 5:12618
- Fasano A, Aquino CC, Krauss JK, Honey CR, Bloem BR (2015) Axial disability and deep brain stimulation in patients with Parkinson disease. *Nat Rev Neurol* 11(2):98–110
- Feng L, Liu TT, Ye DW, Qiu Q, Xiang HB, Cheung CW (2014) Stimulation of the dorsal portion of subthalamic nucleus may be a viable therapeutic approach in pharmacoresistant epilepsy: a virally mediated transsynaptic tracing study in transgenic mouse model. *Epilepsy Behav* 31:114–116
- Guo DQ, Wu SD, Chen MM, Perc M, Zhang YS, Ma JI, Cui Y, Xu P, Xia Y, Yao DZ (2016b) Regulation of irregular neuronal firing by autaptic transmission. *Sci Rep* 6:26096
- Guo H, Zhang H, Kuang Y, Wang C, Jing X, Gu J, Gao G (2014) Electrical stimulation of the substantia nigra pars reticulata (SNr) suppresses chemically induced neocortical seizures in rats. *J Mol Neurosci* 53(4):546–552
- Guo DQ, Chen MM, Perc M, Wu SD, Xia C, Zhang YS, Xu P, Xia Y, Yao DZ (2016a) Firing regulation of fast-spiking interneurons by autaptic inhibition. *Europhys Lett EPL* 114(3):30001
- Handforth A, DeSalles AAF, Krahl SE (2006) Deep brain stimulation of the subthalamic nucleus as adjunct treatment for refractory epilepsy. *Epilepsia* 47(7):1239–1241
- Hu B, Wang QY (2015) Controlling absence seizures by deep brain stimulus applied on substantia nigra pars reticulata and cortex. *Chaos Solitons Fractals* 80:13–23
- Hu B, Guo DQ, Wang QY (2015) Control of absence seizures induced by the pathways connected to SRN in corticothalamic system. *Cogn Neurodyn* 9(3):279–289
- Hu B, Chen S, Chi HM, Chen J, Yuan PP, Lai HH, Dong WY (2017) Controlling absence seizures by tuning activation level of the thalamus and striatum. *Chaos Solitons Fractals* 95:65–76
- Krishna V, Lozano AM (2014) Brain stimulation for intractable epilepsy: anterior thalamus and responsive stimulation. *Ann Indian Acad Neurol* 17(Suppl 1):S95
- Krishna V, King NKK, Sammartino F, Strauss I, Andrade DM, Wennberg RA, Lozano AM (2016) Anterior nucleus deep brain stimulation for refractory epilepsy: insights into patterns of seizure control and efficacious target. *Neurosurgery* 78(6):802–811
- Krishnamurthi N, Mulligan S, Mahant P, Samanta J, Abbas JJ (2012) Deep brain stimulation amplitude alters posture shift velocity in Parkinson's disease. *Cogn Neurodyn* 6(4):325–332
- Lee KJ, Jang KS, Shon YM (2006) Chronic deep brain stimulation of subthalamic and anterior thalamic nuclei for controlling refractory partial epilepsy. In: *Advances in functional and reparative neurosurgery*. Springer Vienna, pp 87–91
- Lehtimäki K, Möttönen T, Järventausta K, Katiskoc J, Tähtinen T, Haapasalo J, Niskakangasa T, Kiekarad T, Öhmana J, Peltola J (2016) Outcome based definition of the anterior thalamic deep brain stimulation target in refractory epilepsy. *Brain Stimul* 9(2):268–275
- Loiseau P, Duche B, Pdespan JM (1995) Absence epilepsies. *Epilepsia* 36(12):1182–1186
- Marescaux C, Vergnes M (1995) Genetic absence epilepsy in rats from Strasbourg (GAERS). *Ital J Neurol Sci* 16:113–118
- Marten F, Rodrigues S, Benjamin O, Richardson MP, Terry JR (2009a) Onset of polyspike complexes in a mean-field model of human electroencephalography and its application to absence epilepsy. *Philos Trans R Soc A Math Phys Eng Sci* 367(1891):1145–1161
- Marten F, Rodrigues S, Suffczynski P, Richardson MP, John R (2009b) Derivation and analysis of an ordinary differential equation mean-field model for studying clinically recorded epilepsy dynamics. *Phys Rev E* 79(2):021911
- Meeren H, van Luijelaar G, da Silva FL, Coenen A (2005) Evolving concepts on the pathophysiology of absence seizures: the cortical focus theory. *Arch Neurol* 62(3):371–376
- Paz JT, Huguenard JR (2015) Microcircuits and their interactions in epilepsy: is the focus out of focus? *Nat Neurosci* 18(3):351–359
- Paz JT, Bryant AS, Peng K, Fenno L, Yizhar O, Frankel WN, Deisseroth K, Huguenard JR (2011) A new mode of corticothalamic transmission revealed in the Gria4-/- model of absence epilepsy. *Nat Neurosci* 14(9):1167–1173
- Paz JT, Davidson TJ, Frechette ES, Delord B, Parada I, Peng K, Deisseroth K, Huguenard JR (2013) Closed-loop optogenetic control of thalamus as a tool for interrupting seizures after cortical injury. *Nat Neurosci* 16(1):64–70
- Pinault D, O'Brien TJ (2005) Cellular and network mechanisms of genetically-determined absence seizures. *Thalamus Relat Syst* 3(3):181
- Rahman M, Abd-El-Barr MM, Vedam-Mai V, Foote KD, Murad GJA, Okun MS, Roper SN (2010) Disrupting abnormal electrical activity with deep brain stimulation: is epilepsy the next frontier? *Neurosurg Focus* 29(2):E7
- Rektor I, Tomck J, Mikl M, Marecek R, Brzdil M, Rektorov I (2013) Association between the basal ganglia and large-scale brain networks in epilepsy. *Brain Topogr* 26(2):355–362
- Roberts JA, Robinson PA (2008) Modeling absence seizure dynamics: implications for basic mechanisms and measurement of thalamocortical and corticothalamic latencies. *J Theor Biol* 253(1):189–201
- Robinson PA, Rennie CJ, Wright JJ, Bourke PD (1998) Steady states and global dynamics of electrical activity in the cerebral cortex. *Phys Rev E* 58(3):3557
- Robinson PA, Rennie CJ, Wright JJ, Bahramali H, Gordon E, Rowe DL (2001) Prediction of electroencephalographic spectra from neurophysiology. *Phys Rev E* 63(2):021903
- Robinson PA, Rennie CJ, Rowe DL (2002) Dynamics of large-scale brain activity in normal arousal states and epileptic seizures. *Phys Rev E* 65(4):041924
- Robinson PA, Rennie CJ, Rowe DL, O'Connor SC (2004) Estimation of multiscale neurophysiologic parameters by electroencephalographic means. *Hum Brain Mapp* 23(1):53–72
- Rodrigues S, Terry JR, Breakspear M (2006) On the genesis of spike-wave oscillations in a mean-field model of human thalamic and corticothalamic dynamics. *Phys Lett A* 355(4):352–357
- Rodrigues S, Barton D, Szalai R, Benjamin O, Richardson MP, Terry JR (2009) Transitions to spike-wave oscillations and epileptic dynamics in a human cortico-thalamic mean-field model. *J Comput Neurosci* 27(3):507–526
- Rubin JE, Terman D (2004) High frequency stimulation of the subthalamic nucleus eliminates pathological thalamic rhythmicity in a computational model. *J Comput Neurosci* 16(3):211–235
- Schtt M, Claussen JC (2012) Desynchronizing effect of high-frequency stimulation in a generic cortical network model. *Cogn Neurodyn* 6(4):343–351
- Shan B, Wang J, Deng B, Wei XL, Yu HT, Li HY (2015) UKF-based closed loop iterative learning control of epileptiform wave in a neural mass model. *Cognitive Neurodynamics* 9(1):31C40
- Shimo Y, Natori S, Oyama G, Nakajima M, Ishii H, Arai H, Hattori N (2014) Subthalamic deep brain stimulation for a Parkinson's disease patient with duplication of SNCA. *Neuromodul Technol Neural Interface* 17(1):102–103
- Slaght SJ, Paz T, Mahon S, Maurice N, Charpier S, Deniau JM (2002) Functional organization of the circuits connecting the cerebral cortex and the basal ganglia: implications for the role of the basal ganglia in epilepsy. *Epileptic Disord* 4(3):9–22
- Sorokin JM, Davidson TJ, Frechette E, Abramian AM, Deisseroth K, Huguenard JR, Paz JT (2017) Bidirectional control of

- generalized epilepsy networks via rapid real-time switching of firing mode. *Neuron* 93(1):194–210
- Sweet JA, Walter BL, Gunalan K, Chaturvedi A, McIntyre CC, Miller JP (2014) Fiber tractography of the axonal pathways linking the basal ganglia and cerebellum in Parkinson disease: implications for targeting in deep brain stimulation. *J Neurosurg* 120(4):988–996
- Takeshita D, Sato YD, Bahar S (2007) Transitions between multi-stable states as a model of epileptic seizure dynamics. *Phys Rev E* 75(5):051925
- Taylor PN, Wang Y, Goodfellow M, Dauwels J, Moeller F, Stephani U, Baier G (2014) A computational study of stimulus driven epileptic seizure abatement. *PLoS ONE* 9(12):e114316
- Taylor PN, Thomas J, Sinha N, Dauwels J, Kaiser M, Thesen T, Ruths J (2015) Optimal control based seizure abatement using patient derived connectivity. *Front Neurosci* 9:202
- van Albada SJ, Robinson PA (2009b) Mean-field modeling of the basal ganglia thalamocortical system. I: firing rates in healthy and parkinsonian states. *J Theor Biol* 257(4):642–63
- van Albada SJ, Gray RT, Drysdale PM, Robinson PA (2009a) Mean-field modeling of the basal ganglia-thalamocortical system. II: dynamics of parkinsonian oscillations. *J Theor Biol* 257(4):664–88
- Volman V, Perc M (2010) Fast random rewiring and strong connectivity impair subthreshold signal detection in excitable networks. *N J Phys* 12(4):043013
- Volman V, Perc M, Bazhenov M (2011) Gap junctions and epileptic seizures—two sides of the same coin? *PLoS ONE* 6(5):e20572
- Vonck K, Sprengers M, Carrette E, Dauwe I, Miatton M, Meurs A, Goossens L, Herdt VD, Achten R, Thiery E, Raedt R, Roost DV, Boon P (2013) A decade of experience with deep brain stimulation for patients with refractory medial temporal lobe epilepsy. *Int J Neural Syst* 23:1250034
- Wichmann T, DeLong MR (2016) Deep brain stimulation for movement disorders of basal ganglia origin: restoring function or functionality? *Neurotherapeutics* 13(2):264–283
- Wilson MT, Sleight JW, Steyn-Ross DA, Steyn-Ross ML (2006) General anesthetic-induced seizures can be explained by a mean-field model of cortical dynamics. *J Am Soc Anesthesiol* 104(3):588–593
- Yi GS, Wang J, Deng B, Wei XL (2017) Complexity of resting-state EEG activity in the patients with early-stage Parkinson's disease. *Cogn Neurodyn* 11(2):147C160